Journal of Atomic, Molecular, Condensed Matter & Nano Physics
Vol. 8, No. 2, pp. 95–112, 2021
ISSN 2582-8215
Published by RGN Publications

http://www.rgnpublications.com

DOI: 10.26713/jamcnp.v8i2.1579

Research Article

Structural, Morphological and Photoluminescence Spectroscopy Studies of Intense Blue Ce^{3+}-doped Lutetium Oxyorthosilicate Scintillator Nanomaterials

M. S. E. Hamroun[1,3], L. Guerbous*[2], K. Bachari[1], M. Taibeche[2], R. Chebout[1], L. Mechernene[3] and A. Nedjar[4]

[1] *Centre de Recherche Scientifique et Technique en Analyses Physico-Chimiques, BP 384, Zone Industrielle, Bou-Ismail CP 42004, Tipaza, Algeria*
[2] *Physics Laser Department/Division of Physics/Nuclear Research Centre of Algiers (CRNA), 02 Boulevard Frantz Fanon, P.O. Box. 399, 16000 Algiers, Algeria*
[3] *Macromolecular Research Laboratory, Faculty of Sciences, Abou Bekr Belkaid University, Chetouane, P.O. Box 119, 13000 Tlemcen, Algeria*
[4] *Nuclear Research Center of Draria, BP 43, Sebala, Alger, Algeria*
***Corresponding author:** guerbous@yahoo.fr

Received: May 8, 2021 **Accepted:** July 21, 2021

Communicated by: M. S. Gupta

Abstract. Monoclinic Lu_2SiO_5(LSO):Ce^{3+} type oxyorthosilicates nanopowders were prepared by sol-gel route. The goal of present work is the study the influence of annealing temperature treatment, up to 1100 °C, on the structural, morphology and photoluminescence properties of LSO:Ce^{3+} nanophosphor. The powder samples were characterized by X-ray diffraction (XRD), field emission-scanning electron microscopy (FE-SEM), Room temperature Raman spectroscopy and room temperature photoluminescence spectroscopy. It was found that the annealing temperature treatment has an effect on the phase purity, the morphology as well as photoluminescence characteristics LSO:Ce^{3+} nanophosphor. An intense violet-blue asymmetric emission band ranged from 370 nm to 470 nm with a maximum intensity situated at around 420 nm, assigned to the 5d→4f ($^2F_{5/2}$,$^2F_{7/2}$) interconfigurational transitions of Ce^{3+} ion in LSO nanomaterial has been observed. Furthermore, LSO:Ce^{3+} present higher emission intensity for sample annealed at 1200 °C. The influences of the presence of LPS, as parasitic phase, on structural, morphological and luminescence properties LSO:Ce^{3+} nanomaterial were highlighted. Also, using the experimental data and wave function-based *ab-initio* calculation results, the Ce^{3+} energy levels position relative to the LSO nanomaterial band structure were found.

Keywords. Ce^{3+}; Lutetium oxyorthosilicate; Sol gel; Nanophosphors; Photoluminescence

PACS. 78.55.Qr

1. Introduction

Cerium-doped lutetium silicates Lu_2SiO_5 (LSO) and $Lu_2Si_2O_7$ (LPS) meet the required criteria for gamma rays detection scintillators. Since its discovery by Melcher and Schweitzer in 1992 [23,24], lutetium orthosilicate Lu_2SiO_5 (LSO) is of great interest as a scintillating material. In fact, this material doped with Ce^{3+} ions give a scintillator which exhibits a high scintillation efficiency (273,300 photons/MeV), a short decay time (~40 ns) and a high density (7.4 g/cm^3) [31]. These properties are of particular interest for medical imaging applications and other fields. LSO appears to be a promising scintillator. We now replace BGO, a classical scintillator, in positron emission tomography (PET). Generally, LSO is prepared as a single crystal, but it is difficult to produce a high-quality single crystal and the maximum achievable concentration of ionic doping is quite low. However, the LPS ($Lu_2Si_2O_7$) type compositions have the disadvantage of a lower stopping power than those of the LSO or LYSO type [11].

Moreover, today there is an immense attempt to control rare earth ions doped inorganic nanomaterial [10]. It is known that the performances of nanocrystals (NCs) are different from those of the same bulk materials. Consequently, controlling the crystallographic structure, crystallite size and shape parameters is a fundamental and technological importance. In fact, it exists a strong relation between these parameters and the electronic, magnetic and optical properties of these nanomaterial. In addition, the enhancement in the emission intensity is an important aspect for the development of luminescent devices. Furthermore, it is well known that the structural and optical properties of a material depend on the preparation methods. If the absorption and luminescence spectra of $Lu_2SiO_5:Ce^{3+}$ single crystal were well measured and investigated in numerous papers [14, 38], the control of structural and optical parameters of same material in nanoscale is remains still a challenge. Indeed, nowadays, Ce^{3+}-doped Lu_2SiO_5(LSO) nanophosphors in several shapes and sizes have been already prepared by a variety of methods, such as solid-state reaction, hydrothermal precipitation and Pechini method [30]. While the sol gel method is most commonly used for the synthesis of nanomaterials with high homogeneity and purity, it allows controlling the size and morphology of the particles, not requiring high-temperature heat treatment [15]. However, the difficult is the control the final oxyorthosilicate products in terms of crystalline phase purity. The oxyorthosilicate LSO crystallizes in monoclinic structure with space group C2/c; Lu ions occupy two crystallo graphically inequivalent cation sites with coordination number 6 or 7. The lutetium ions occupy two crystallographic sites Lu_1 and Lu_2 with low symmetry (C_1) and with seven and six oxygen neighbors, respectively [27]. Lu_1 site presents distances Lu-O varies between 2.16 and 2.34 Å and the seventh oxygen is at 2.61 Å corresponding to a larger site.For Lu_2 site, the Lu-O distance ranges from 2.16 to 2.24 Å. On the other hand, the oxyorthosilicate LPS crystallizes in monoclinic symmetry with space group C2/m. This lattice exhibits a single crystallographic site for lutetium ions, with six oxygen neighbors forming a distorted octahedron with C_2 point symmetry [27]. Furthermore, it is known that the emission of Ce^{3+} in LPS is blue shifted than that of in LSO [26] and that of LPS or LSO nanomaterials is red shifted than that of their corresponding

single crystals. Consequently, the investigation and the discussion of the photoluminescence spectra in LSO in presence of LPS are complicated. Although, in many papers, rare earths doped LSO and LPS pure phases are studied, the influence of the presence of one phase in the other as parasite has not been evaluated. In this paper, we report high blue emission $Lu_2SiO_5:Ce^{3+}$ nanophosphors synthesized by sol gel method. Furthermore, the present work also aims to study and assess the influence of the presence of LPS, as parasitic phase,on LSO nanomaterial properties prepared by sol gel method. The effect of annealing temperature on the structural, morphological and luminescence spectroscopy properties of Ce^{3+}-doped LSO in presence of LPS phase were highlighted. Also, Vienna Ab-initio Simulation Package (VASP) was used to perform the first principle calculation of Ce^{3+}-doped LSO nanomaterial.

2. Experimental

2.1 Samples Preparation

The Lu_2SiO_5: 1 at % Ce^{3+} ($Lu_{1.98}Ce_{0.02}SiO_5$) powders samples were prepared by sol–gel method. The Lutetium oxide (Lu_2O_3, 99,999 %, Fluka Chemika) and cerium (III) nitrate hexahydrate ($Ce(NO_3)_3.6H_2O$, 0, 99 %, Biochem Chemopharma) were dissolved in 100 ml of deionized water and 3 ml of nitric acid (HNO3). After the mixed solution was stirred at room temperature, we add tetraethyl orthosilicate (TEOS, $SiC_8H_{20}O_4$, 99.0 %, Sigma-Aldrich) precursor of silicate. In the resulting solution, we added an organic complex Ethylene glycol (Fluka) in 1 : 1 mass ratio to the expected mass of the final product and stirred for 1 h at room temperature. The pH was adjusted to 7 by slowly adding ammonia solution and stirring until gel was obtained. Drying is performed at 120 °C for 2 days. Finally, the powders were introduced in a furnace and heated in air at different temperature 1100, 1200, 1300, 1400 °C during 4 h for each sample.

2.2 Characterization

The phase identification and the related properties of the nanopowders were investigated by X-ray diffraction (XRD) technique a PAN analytical X'Pert (Philips) PRO using CuKα radiation ($\lambda = 1.54059$ Å) operated at 45 kV and 40 mA. A symmetric (θ-θ) scans were performed from 10 ° to 90 ° 2θ with a step width of 0.02°. All the data were processed by X'Pert High Score plus Software with commercial databases (FWHM deduction and peak identification). The morphology of the powders has been studied by scanning electron microscopy (SEM) (SEM, Philps XL-30). The evolution of the powder of the $Lu_2SiO_5:Ce^{3+}$ from the amorphous state (xerogel) to the crystalline state was studied by Differential scanning calorimetry DSC (DSC SetsysEv1500c). The room temperature Raman spectra were recorded by HORIBA (iHR 320).

The photoluminescence spectra were carried out using Perkin-Elmer (LS-50B) luminescence spectrometer using Xe lamp with excitation wavelength at room temperature as described in ref. [9]. Before the deconvolution, the room temperature emission spectra are plotted as relative emitted energy per constant energy interval, recommended for broad emission bands, as described in ref. [35].

3. Results and Discussion

3.1 Thermal Analysis DSC

To get information on the crystallization of lutetium orthosilicate, the evolution of the xerogel powder in amorphous state to the crystalline state was studied by DSC thermal analysis. As shown in Figure 1, the first endothermic peaks observed in the 140-203 °C temperature range are attributed to the elimination of adsorbed species, such as water or alcohol molecules [8]. The other peaks observed at about 360-500 °C are attributed to the decomposition of nitrates and organic radicals. The last exothermic peak strongly observed at 1000 °C corresponds to the crystallization of the amorphous Si–O–Lu solid network getting LSO material and LPS as parasitic phases.

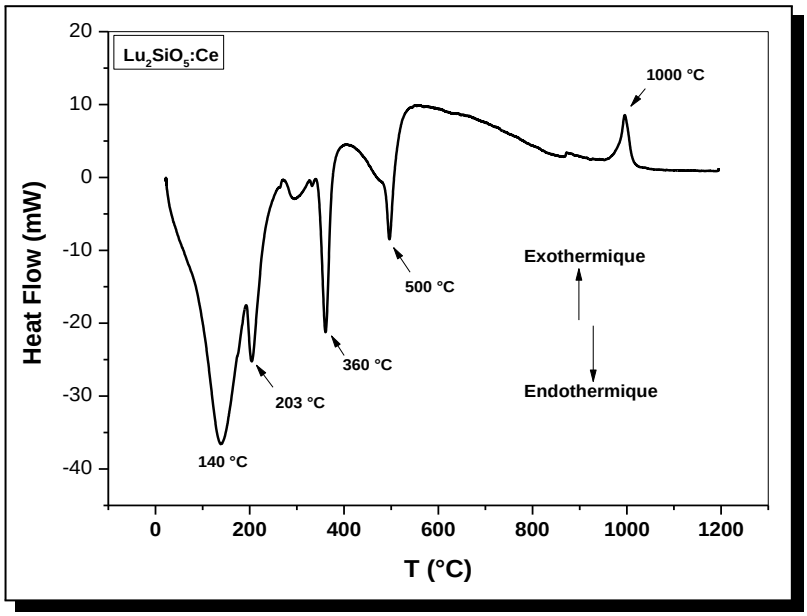

Figure 1. Differential scanning calorimetry (DSC) spectra of a xerogel $Lu_2SiO_5 : Ce^{3+}$

3.2 XRD Analysis

The superposed diffractograms in Figure 2 show the results of XRD analysis on samples of Ce^{3+} doped Lu_2SiO_5 annealed at different temperatures 1100, 1200, 1300 and 1400 °C, which have a monoclinic C2/c structure (JCPDS No. 00-041-0239). It is noted that at a temperature of 1100 °C a crystallization of the powder with the structure Lu_2SiO_5 is observed. At the annealing temperature of 1200 °C, all diffraction peaks become sharper and stronger due to the increase in the crystallinity and the growth of the crystallite size. We have peaks of the parasite phase $Lu_2Si_2O_7$(LPS) (JCPDS No. 00-35-0326) with the monoclinic structure on the XRD diffractogram of the samples. These peaks are more pronounced, intense and numerous in the case of the annealed powders at 1100 °C and 1400 °C and less in the sample annealed at 1300 °C. For the sample fired at 1200 °C, there is only one peak corresponding to this parasite phase $Lu_2Si_2O_7$ (LPS), which the purest sample of phase point of view compared to the others annealing temperature.

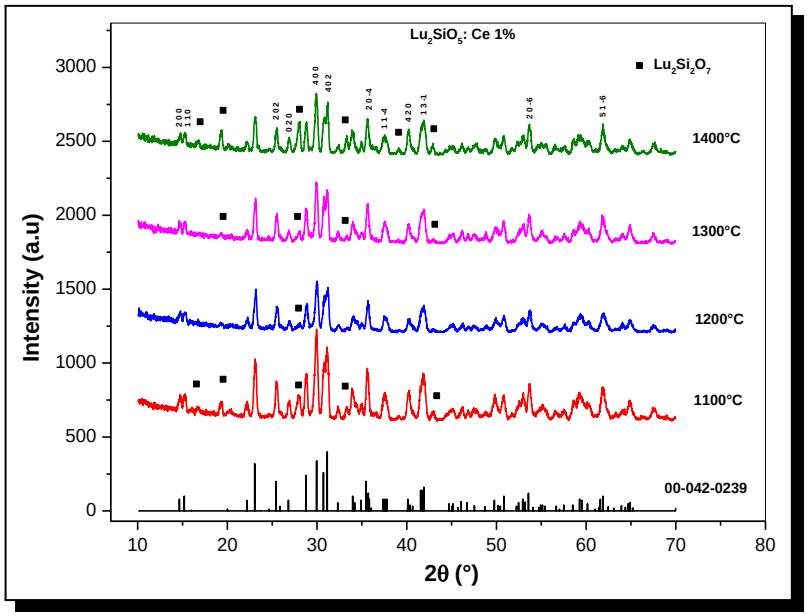

Figure 2. XRD diffractogram of $Lu_2SiO_5 : Ce^{3+}$ samples powders annealing at different temperatures 1100, 1200, 1300, 1400 °C

We have performed the calculations of the crystallite size and lattice parameters for each type of powder sample. The significance of the broadening of peaks evidences grain refinement along with the large strain associated with the powder. The instrumental broadening (β_{hkl}) was corrected, corresponding to each diffraction peak of material using the relation:

$$\beta_{hkl} = \left[(\beta_{hkl})^2_{\text{Measured}} - (\beta_{hkl})^2_{\text{Instrumental}}\right]^{\frac{1}{2}}. \tag{3.1}$$

The average nanocrystalline size was calculated using Debye-Scherrer's formula:

$$D_{sh} = \frac{k\lambda}{\beta_{hkl}\cos\theta}, \tag{3.2}$$

where β_{hkl} is the full half width maximum (FWHM) of the pure diffraction profile in radians, k is shape factor (0.9), λ is the wavelength of the X-rays (0.154056 nm), θ is the diffraction angle, and D_{hkl} is the average diameter of the crystallite. The average crystallite size (D_{sh}) and crystallographic parameters are calculated and listed in Table 1. It is known that β_{hkl}, in the Scherrer formula, can be interpreted in terms of lattice strain and crystalline size. The crystal lattice strain generated by the annealing temperature is determined from the Williamson-Hall relationship [36]:

$$\beta_{hkl}\frac{\cos\theta}{\lambda} = \frac{1}{D_{\text{W-H}}} + \frac{\eta\sin\theta}{\lambda}, \tag{3.3}$$

where $D_{\text{W-H}}$ is the effective crystallite size on Williamson-Hall model and η is the effective strain. The strain is calculated from the slope of the plot of $\beta((\cos\theta)/\lambda)$ against $(\sin\theta)/\lambda$ and the effective crystallite size for each sample is calculated from the intercept to $\beta((\cos\theta)/\lambda)$ axis as shown in Figure 3. In Table 1, we present the cell parameters of LSO: Ce^{3+}. We can note that the sample annealed at 1200 °C presents the larger mesh size (V = 822.9 Å^3) and the highest strain value compared to other firing temperature. This phenomenon can, be related

to the presence degree of LPS as parasitic phase in final material. One can thought that more homogenous crystallitesbelong to the LSO phase, at 1200 °C, leads to a large interaction surface, which increases the strain, however, the LPS parasite phase reduced these surfaces. In addition, one can observe that the crystallite size calculated with both the Williamson-Hall and Scherrer methods increases from 1100 °C to a higher value, roughly constant for annealed samples at 1200 °C, 1300 °C and 1400 °C.

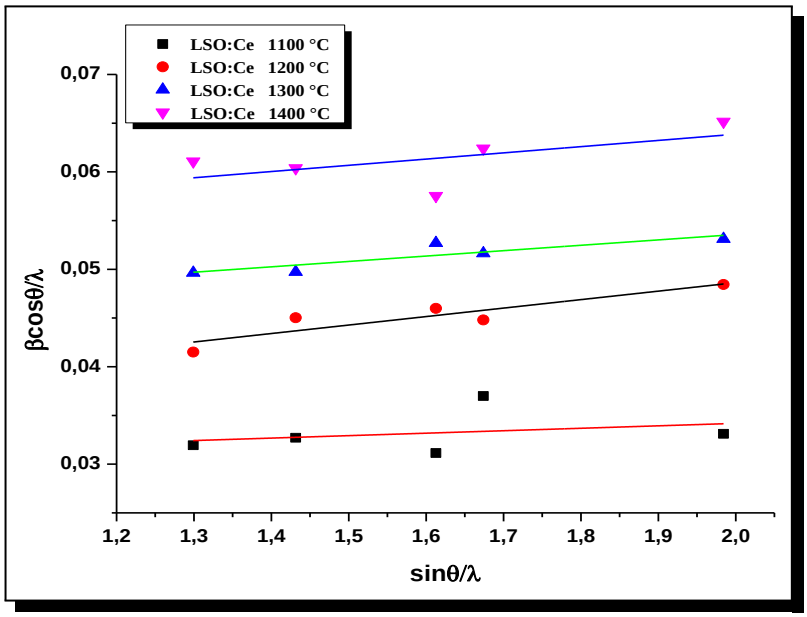

Figure 3. Williamson-Hall Analyze of $Lu_2SiO_5:Ce^{3+}$ annealed at different temperatures. The lines obtained are plotted after adjustment of the experimental points

Table 1. Grain size and crystallographic parameters of the samples of $Lu_2SiO_5:Ce^{3+}$

	a(Å)	**b(Å)**	**c(Å)**	**V(Å^3)**	**β(°)**	**D_{sh}(nm)**	**D_{w-h}(nm)**	**ξ**
LSO : Ce 1100 °C	12.31	6.64	10.26	816.8	103.12	35	34	0.0025
LSO : Ce 1200 °C	12.33	6.66	10.26	822.9	102.68	39	47	0.0087
LSO : Ce 1300 °C	12.31	6.64	10.25	815.97	102.99	37	44	0.0055
LSO : Ce 1400 °C	12.3	6.64	10.21	813.27	102.96	42	47	0.0063

To describe approximately the growth rate of nano-crystals during the thermal annealing of Ce^{3+}-doped both LSO and the parasitic LPS phases, reference is made to the Scott equation [19] given below under the growth conditions of the nano-crystallites

$$D = C\exp\left(\frac{-E}{RT}\right), \tag{3.4}$$

where D is the crystallites size, C is a constant obtained after adjusting the straight lines of the curve $\ln(D) = f(1000/T)$, E is the crystal growth activation energy (Scott energy), R is the ideal gas constant ($R = 8.314$ J K^{-1} mol^{-1}) and T is the absolute temperature.

From the equation (3.4), we can arrive at the equation of the straight-line $\ln(D) = f(1000/T)$.

$$\ln(D) = \ln(C) + \left(\frac{-E}{R\,1000}\right)\left(\frac{1000}{T}\right). \tag{3.5}$$

From the equation (3.5) the energy of Scott can be derived after calculation of the slope of the straight lines of the curve $\ln(D) = f(1000/T)$ (Figure 4) for each temperature interval. According to the XRD patterns of the Ce^{3+} doped Lu_2SiO_5 samples (Figure 1), it is also noted that there is a parasitic phase of $Lu_2Si_2O_7$ and also evolves with the annealing temperature. For this purpose, to understand the phenomenon that takes place, we have been able to calculate the grain sizes of this parasitic phase for each annealing temperature.

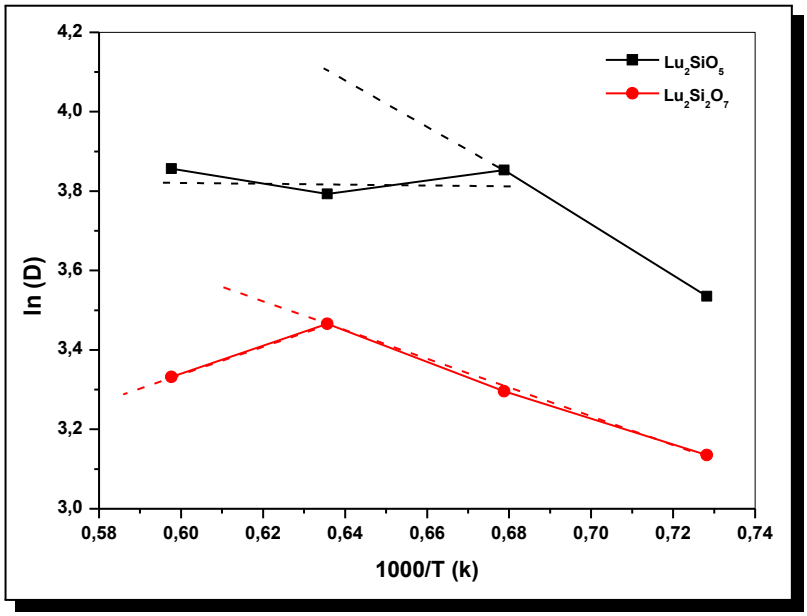

Figure 4. Scott energy curves of LSO and LPS

In the temperature range 1100-1200 °C; the activation energy of the structure LSO is $E_{\text{Scott}} = 53.459$ kJ/mol and for the interval 1100-1300 °C, the activation energy of the LPS structure is 29.579 kJ/mol. From these two values, it can be said that in this temperature range the crystal growth of the LSO phase is faster than that of the parasitic phase LPS one. In the temperature range 1200-1400 °C; the activation energy of the Lu_2SiO_5 structure is of low E_{Scott} value = 79 J/mol. In this case, it is deduced that the growth has become smaller and smaller, which corresponds to values of the crystallite sizes which are almost constant. The energy decreases in the case of parasitic phase $Lu_2Si_2O_7$ which has a negative value, it can be said that the sample promotes the structure Lu_2SiO_5 and the parasitic phase $Lu_2Si_2O_7$ has been decomposed.

3.3 Raman Spectroscopy

Figure 5 illustrates the room temperature unpolarized Raman spectra of $Lu_2SiO_5:Ce^{3+}$ powders annealed at two different temperature 1200 °C and 1400 °C for 4 h. For LSO phase, the irreducible point representations of C2/c symmetry group allow 96 Raman active vibrational modes (on a total of 192) with 48 Ag and 48 Bg [6, 29]. Furthermore, there were identified 24Ag+24Bg vibrations at room temperature in the Raman spectra of the LSO crystal structure [33].

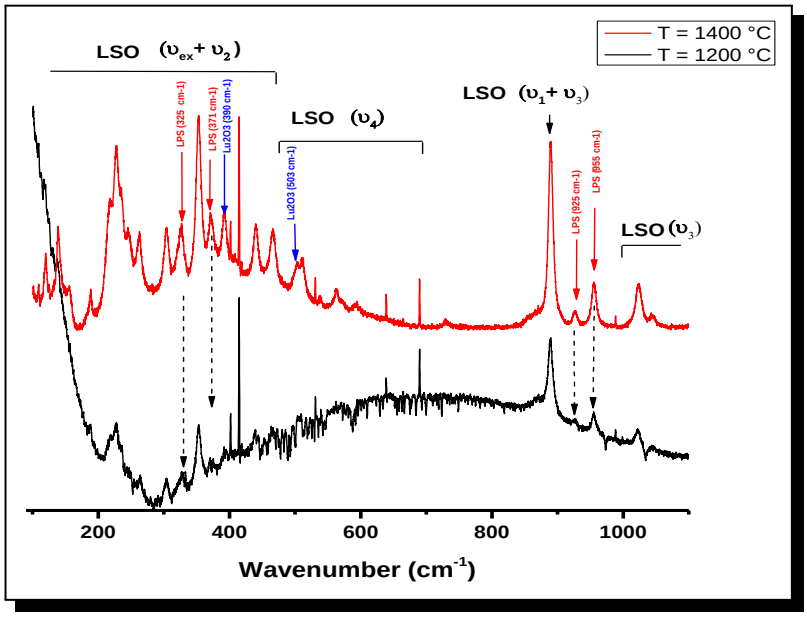

Figure 5. Raman spectra of $Lu_2SiO_5:Ce^{3+}$ powders annealed at 1100 °C and 1400 °C

The spectra present a number of vibrational modes belonging to the B-centred monoclinic unit cell (C2/c space group) of oxyorthosilicate crystals with smaller trivalent rare earth ionic radius and the maxima are well match those reported for the LSO material published in the literature [33]. It is known that the vibrational transitions of Lu_2SiO_5 (LSO) can be divided into three different regions, namely as indicated on the figure: (i) the low-wavenumber range below 300 cm^{-1} which is connected with cation motions (lattice vibrations), (ii) the range between 300 and 600 cm^{-1} related to RE-O stretching (Lu-O) and SiO_4 bending vibrations, and (iii) the high wave number range between 800 and 1060 cm^{-1} in which SiO_4 symmetric and anti-symmetric stretching vibrations appear [37]. As seen on Figure 5, the peaksrelated to LSO in the regions namely: below 440 cm^{-1}, 450-690 cm^{-1} and 891-914 cm^{-1} were assigned to the $(\nu_{ext}+\nu_2)$, (ν_4) and $(\nu_1+\nu_3)$ vibrations respectively [33]. Increasing the annealing temperature, the two spectra present similar features,in which all the frequency peaks of LSO vibrational modes present at 1200 °C were observed for 1400 °C. Furthermore, the intensity of this band is remarkably improved by the increasing the temperature from 1200 to 1400 °C. It is clear that when the temperature is increased, the peaks of vibration of the bonds become much more intense and sharper, indicating that the crystallinity becomes much better and the crystallite size increases.

Some LPS parasitic phase peaks exist with very weak intensities for 1200 °C as indicated on Figure 5 by broken arrows situated at 325, 371, 925 and 955 cm^{-1} [34]. The LPS Raman peaks, indicated by red arrows on Figure 5, become narrower and more intense for 1400 °C annealing temperature. In addition to the vibrational modes of the LSO crystalline structure and LPS parasitic phase at 1400 °C, additional peaks were observed at 390 cm^{-1} and at 503 cm^{-1}, indicated by blue arrow, which should be assigned to the cubic Ia3 Lu_2O3 crystalline phase and which is not exist at 1200 °C [28]. It is important to note that the presence of the Lu_2O_3 as a parasitic phase will decrease the emission efficiency of Ce^{3+} in oxyorthosilicate.

3.4 Morphology

In order to determine the influence of heat treatment and to assess the influence of the presence of LPS parasitic phase on the morphology of particles formed, we performed a SEM analysis under enlargements 5 μm. Figure 6(a-d) illustrates the morphology of 1% Ce^{3+} doped lutetium silicate powders non-annealed and annealed at 1100, 1200 and 1400 °C for 4 h.

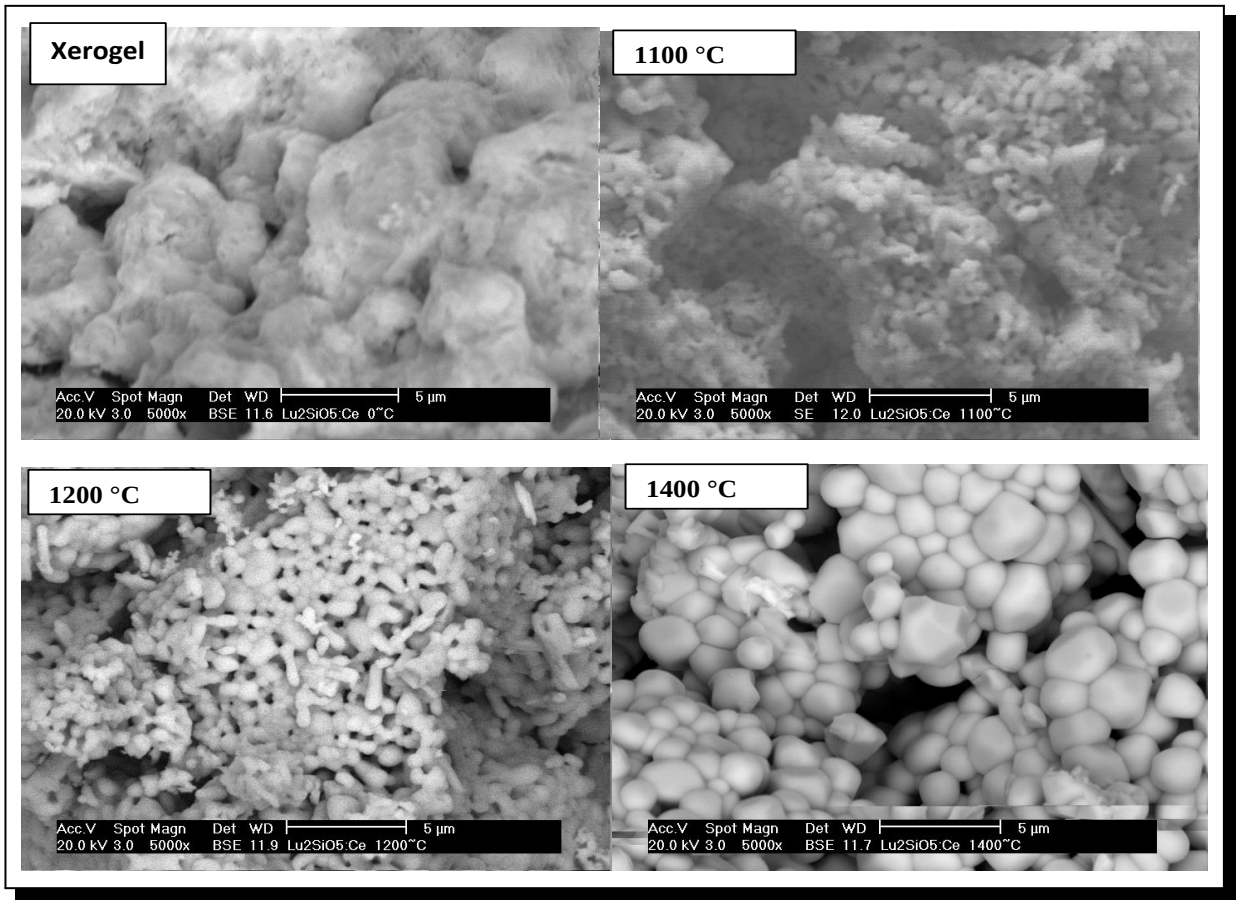

Figure 6. (a-d): Morphology of $Lu_2SiO_5 : Ce^{3+}$ samples annealed at different temperatures: 1100, 1200, 1300, 1400 °C

For the non-annealed sample, it is noted that there is no regular shape or architecture and that is reflected by the amorphous structure of the powder. One can observe that with increasing

of annealing temperature, the particles become biggest with regularly, clearer and shaped form. In addition, we note also that the morphology is influenced by the presence of LPS phase. The sample annealed at 1100 °C, presents a morphology consisting of non-homogenous clear particles with different shapes and small sizes between 0.1 and 0.2 μm. For the sample annealed at 1200 °C, it presents a smooth surface with maximum homogenous and relatively narrow distribution of ellipsoidal shape-like particles. These particles size with about 0.4 μm are larger than those of the previous sample and can be represent the LSO phase with minimum PLS parasitic phase. The morphology of sample annealed at 1400 °C exhibits amicronic networks constitutes with large and non-homogenous highly-facetted primary particles, connected to one another with their smooth surfaces. Furthermore, theses primary particles present different sizes between about 1 μm to 2 μm. One can consider that the difference in shape and size of the particles for 1100 °C and 1400 °C annealing temperatures are due to the presence of LPS parasitic phase. In addition, the particles are constituted from the agglomeration of several crystallites as estimated by W-H method.

3.5 Photoluminescence study

Figure 7(a) shows the emission spectra of 1% Cerium doped Lu_2SiO_5 powders and annealed at different temperatures 1100, 1200, 1300, 1400 °C. The excitation spectra of the samples were made at a wavelength λ_{ex} = 356 nm for each sample and at ambient temperature. All the spectra are marked by an intense band centered on 410 nm, attributed to the emission of cerium in the matrix of lutetium orthosilicates LSO, corresponds evidently to the transition 5d→4f which emits in blue violet. This result is in agreement with that of Mansuy et al. [22] who studied the emission of cerium with different percentage in the Lu_2SiO_5 matrix annealed at 1200 °C prepared by different sol-gel methods and recipes. From Figure 7(a), it can easily be seen that the emission intensity in the case of the annealed sample at 1200 °C is higher compared to the other samples. The emission intensity starts to increase from 1100 to 1200 °C and then decreases. This observation can be related to the purity of LSO phase and the degree of LPS parasitic phase in matrix, in agreement with XRD and morphology analysis.

As it recognizes in XRD analysis, LPS phase coexist with LSO one as parasitic and consequently, the photoluminescence (PL) spectra can be explained in the light of the incorporation of Ce^{3+} ion in the different sites as the structure of orthosilicates change. It is reported that emission of Ce^{3+}-doped LSO is around 420 nm 390 nm [23, 24] and LPS, presents as a parasitic phase, at 385 nm [28], which are generally close. Therefore, it is supposed that Ce^{3+}-doped both LSO and LPS emissions appear in the same spectrum, however, this is not the casein our samples. In fact, only Ce^{3+}-doped LSO emission is present, what makes us to think that Ce^{3+} emission in LPS parasitic phase is quenched; transferred and/or Ce^{3+} ion did not substitute Lu^{3+} in LPS. Furthermore, one can observe that although the Ce^{3+}-doped LPS emission is absent the Ce^{3+}-doped LSO emission intensity depends on the degree of presence LPS phase.

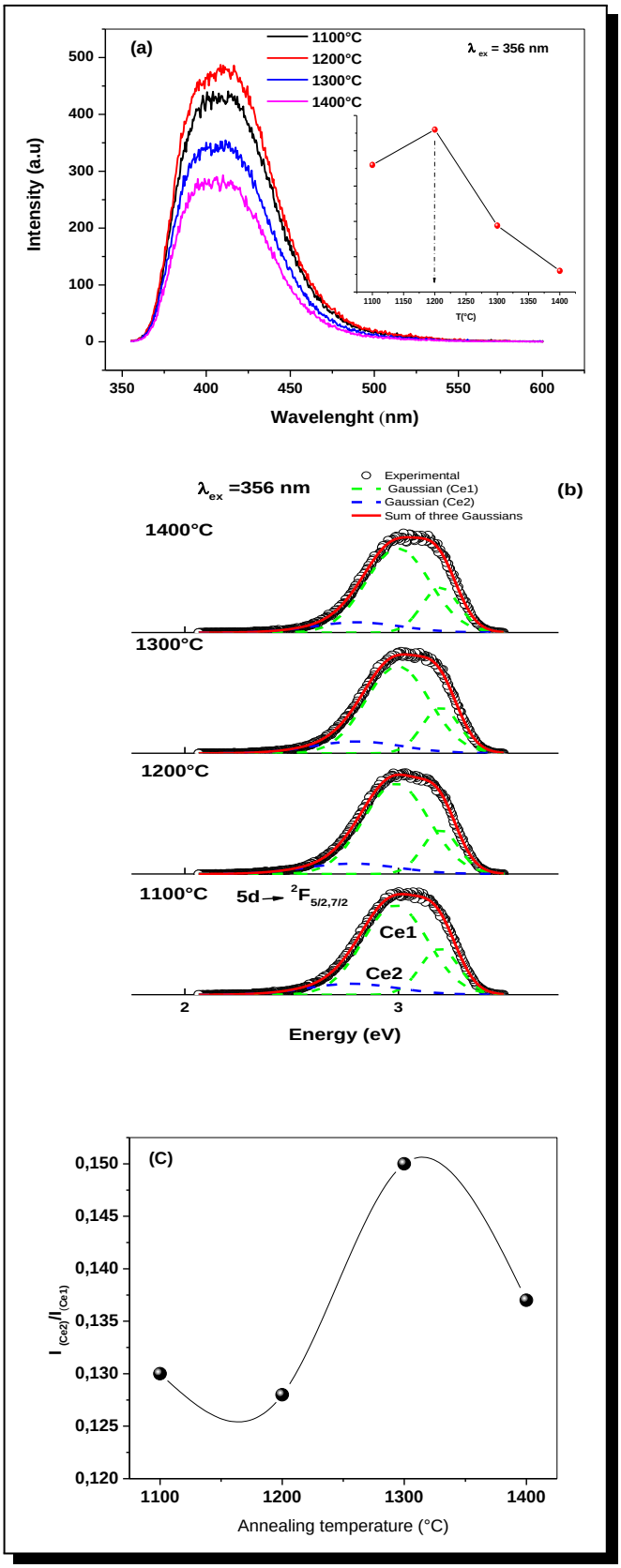

Figure 7. Emission spectra of 1% Cerium doped Lu_2SiO_5 powders annealed at different temperatures: 1100, 1200, 1300, 1400 °C

We thought that LPS parasitic phase may plays a quenching role for Ce^{3+}-doped LSO emission. In the goal to more investigate on the effect of the annealing temperature treatment and the presence of LPS parasitic phase on the luminescence properties, all recorded emission spectra were adjusted by deconvolution processing using Gaussian spectral curves and analyzed. As it is well known that in LSO phase, Ce^{3+} ions reside in both of the two crystallographic distinct Lu sites [4]. A smaller site (Ce_1) in which the Ce^{3+} ions show efficient 5d→4f emission.Otherwise, the luminescence from Ce^{3+} ions occupying the larger Lu sites (Ce_2) is highly quenched at room temperature and appears as a weak shoulder on the weaker energies side of the stronger Ce_1 emission [20]. Indeed, it was found that for all annealing temperature, the emission spectra were well easily adjusted as a sum of three Gaussian bands,as presented in Figure 7(b), as an example. The first and the second Gaussian curves were assigned to the emission of Ce^{3+} in the smaller site (Ce_1) and the third weak one to the larger (Ce_2) [7].

Naud et al. [25] have considered that the integral of the emission intensity from a given type of Ce center is directly proportional to the concentration of that type of Ce center. Consequently, the ratio of the concentrations of the two types of Ce sites is proportional to the ratio of the integrated emission intensities from the two types of Ce sites. In Figure 7(c) we display the variation of the ratio of the integrated intensity of Ce_2 emission to that of Ce_1 $I(Ce_2)/I(Ce_1)$ against the annealing temperature. The emission from Ce_2 site presents weak intensity for the lower annealing temperatures and high for higher temperatures, connected to the degree presence of LPS parasitic phase, independently of crystallite size. One can thought that LPS favors or help Ce^{3+} to occupy the Ce_2 site in LSO phase.

Figure 8(a) shows the excitation spectra measured at 410 nm emission wavelength, corresponding to 5d→4f ($^2F_{5/2}$, $^2F_{7/2}$) interconfigurational transition of Ce^{3+}. The excitation spectra are composed by two absorption bands; a strong broad band localized at around 356 nm and a weak band centered at 297 nm, which can be attributed to transitions from the 4f($^2F_{5/2}$) ground state to the first and second excited level of 5d ($5d_1, 5d_2$) configuration of Ce^{3+} in LSO phase. To careful analysis of the excitation spectra, the $5d_1$ band is well adjusted to two Gaussian curves (Figure 8(b)). The intense higher band situated at longer wavelengths side is associated to Ce_1 and the weaker in side of shortest wavelengths to Ce_2. Consequently, the integrated intensity of each Gaussian presents the excitation efficiency of Ce in such site. The variation of the integrated intensity ratio of Ce_2 to Ce_1 $I(Ce_2)/I(Ce_2)$ is displays on Figure 8(c). One can observe that this ratio decreases from 1100 °C to 1200 °C which presents the smallest value and increases for 1300 °C and 1400 °C. This behavior is connected also to the presence of LPS parasitic phase. One can thought that the LPS parasitic phase favorizes the Ce_2 occupation and therefore the energy transfer from Ce_2 to Ce_1, in agreement with the analysis of emission spectra.

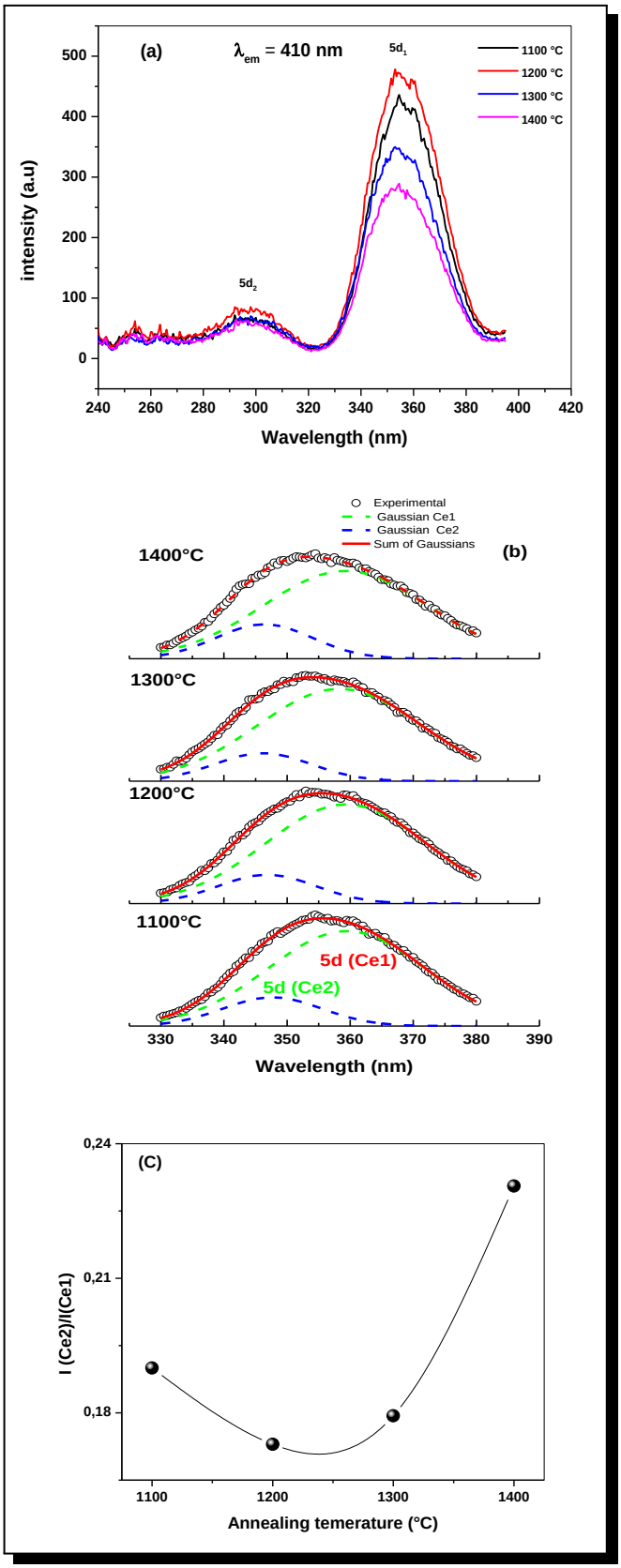

Figure 8. Excitation spectra of 1% Cerium doped Lu_2SiO_5 powders annealed at different temperatures: 1100, 1200, 1300, 1400 °C

The energy difference between the conduction band and 4f group state of Ce^{3+} is a crucial parameter used to construct the energy-level diagram for the 4f ground states and the lowest 5d states of Ce^{3+} relative to LSO host valence and conduction bands. With the availability of the energy-level diagram, we may interpret or even predict optical properties of the ions in a given host. For this goal, we have performed calculations using the Vienna Ab-initio Simulation Package (VASP) [17, 18] based on the density functional theory, the initial atomic positions and symmetry information of the host crystal were taken from Bilbao crystallographic server [2]. The $4f^{14}5p^6 5d^1 6s^2$ electrons on Lu, the $3s^2 3p^2$ electrons on Si, the $2s^2 2p^4$ electrons on O, and the $5s^2 5p^6 4f^1 5d^1 6s^2$ electrons on Ce, were treated as valence electrons. The plane wave cut-off energy for the electronic wave functions was set to 550 eV. The Brillouin zone was sampled with a mesh of $4 \times 4 \times 4$ centered at Gamma point. The total energy convergence criterion was set to 10^{-6} eV and the maximum component of force acting on any atom in the relaxed geometry was less than 0.01 eV/A. For the structural relaxation calculation part, we used the supercell of Lu_2SiO_5 (LSO) $1 \times 2 \times 1$ containing 128 atoms. In addition, the two inequivalent cation sites Lu_1 and Lu_2 were used. The electronic properties were studied using DFT+U to trait the Ce^{3+} 4f levels energy in the host band, and the hybrid DFT with the HSE06 functional to adjust the energy gap of LSO material and also treat the cerium 4f-5d energy levels, HSE06 calculations were performed using the default fraction ($\alpha = 0.25$) of nonlocal Flock exchange [12, 13].

For a very precise modeling of 4f electrons and their interactions, it is necessary to use DFT+U, we found the U_{eff} correction for Ce^{3+}-doped LSO is give reasonable quantitative agreement between theory and experiment results for the energy levels of 4f electrons [1]. Using the rotationally invariant method of Dudarev [5], we calculated the parameter U_{eff} for anonsite+U correction to treat the Ce^{3+} 4f, electrons with a single parameter $U_{eff} = U - J$. The U_{eff} is tuned in such a way to localized 4f state in the band gap of the host estimated at 7.5 eV [32]. This value is closed to the value of the band gap published by Kitaura et al. [16]. In our case, for LSO: Ce^{3+} nanomaterial, it was found that the value of U_{eff} to find the 4f-Cerium orbital in the band gap is equal 3.1 eV as shown in Figure 9. Also, we can see that the 4f ground states is situated at 2.44 eV above the valence band maximum, which can give a partial agreement is with the criteria of the luminescence for the 5d states calculation [3].

In addition, we can complete the 5d schematicenergy levels of Ce^{3+} inside the total density of state TDOS of LSO using the following equation (Figure 9) [8, 32]:

$$Eg = \Delta E_{4f-VBM} + E(Ce^{3+}, LSO) + \Delta E_{5d1-CBM}, \tag{3.6}$$

where $E_{4f-VBM}$is 2.44 eV and the band gap is Eg = 7.5 eV taken from the calculation. E (Ce^{3+}, LSO) = 3.024 eV (410 nm) taken as the maximum emission spectrum band. One can estimate the energy difference between the bottom of the conduction band and the lowest energy level $5d_1 \Delta\ E_{5d1-CBM}$ and the next higher energy level $5d_2$ situated at 2.03 eV and 1.34 eV below the minimum of the conduction band respectively as shown in Figure 9.

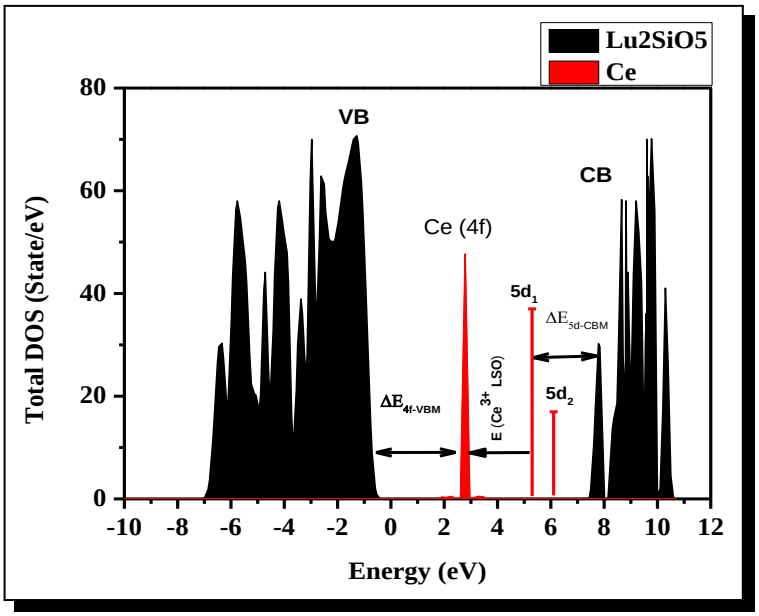

Figure 9. Total density of state of LSO: Ce^{3+}, the schematic diagram of 4f and 5d energy level position relative to band structure are shown

4. Conclusion

In this work, the monoclinic nanocrystalline lutetium oxyorthosilicate Lu_2SiO_5: 1 at % Ce^{3+} powder material has been synthesized by sol gel route. Different LSO: Ce^{3+} samples have been obtained under for annealing temperature namely: 1100, 1200, 1300, 1400 °C for 4h annealing duration. This crystallization temperature was confirmed by thermal analysis (DSC) carried out on a dry gel of LSO: Ce^{3+}. The XRD and Raman analysis shown that the monoclinic LSO phase exist with Lu_2Si2O_7 (LPS) as parasitic phase. SEM analysis reveals the spherical shapes for samples annealed from 1200 °C to 1400 °C. The crystallite size obtained for LSO phase from XRD analysis was found to be in the range of 34-47 nm. All samples present an intense broad blue emission band in the range of 370-470 nm with a maximum intensity at around 410 nm, characteristic of 5d→4f ($^2F_{5/2}$, $^2F_{7/2}$) interconfigurational transition of Ce^{3+} ion in Lu_2SiO_5 nanomaterial. In fact, highly luminescent blue nanophosphors of Ce^{3+}-doped Lu_2SiO_5 were recorded for sample annealed at 1200 °C, which represents the purest sample in term of presence of LPS parasitic phase. Furthermore, our results highlight the role of presence of LPS parasitic phase on the luminescence of Ce^{3+}-doped LSO nanocrystals, and it is found that the photoluminescence process strongly depends on degree of its presence. Furthermore, the present work demonstrates also that by combining the photoluminescence experimental data and that derived from the theoretical simulation namely: the band gap value of LSO as well as 4f position relative to the maximum of valence band, the schematic diagram of 4f and 5d energy level positions relative to band structure was constructed.

Competing Interests

The authors declare that they have no competing interests.

Authors' Contributions

All the authors contributed significantly in writing this article. The authors read and approved the final manuscript.

References

[1] H. A. Badehian, H. Salehi and M. Ghoohestani, First-principles study of elastic, structural, electronic, thermodynamical, and optical properties of Yttria (Y_2O_3) ceramic in cubic phase, *Journal of the American Ceramic Society* **96** (2013), 1832 – 1840, DOI: 10.1111/jace.12259.

[2] Bilbao Crystallographic Server, `http://www.cryst.ehu.es/`, May 2021.

[3] A. Canning, A. Chaudhry, R. Boutchkoand and N. Grønbech-Jensen, First-principles study of luminescence in Ce-doped inorganic scintillators, *Physical Review B – Condensed Matter and Materials Physics* **83** (2011), 125115, DOI: 10.1103/PhysRevB.83.125115.

[4] D. W. Cooke, B. L. Bennett, K. J. McClellan, J. M. Roper, M. T. Whittaker and A. M. Portis, Electron-lattice coupling parameters and oscillator strengths of cerium-doped lutetium oxyorthosilicate, *Physical Review B – Condensed Matter and Materials Physics* **61**(18) (2000), 11973, DOI: 10.1103/PhysRevB.61.11973.

[5] S. L. Dudarev, G. A. Botton, S. Y. Savrasov, C. J. Humphreys and A. P. Sutton, Electron-energy-loss spectra and the structural stability of nickel oxide: An LSDA+U study, *Physical Review B – Condensed Matter and Materials Physics* **57** (1998), 1505, DOI: 10.1103/PhysRevB.57.1505.

[6] A. Ellens, H. Andres, A. Meijerink and G. Blasse, Spectral-line-broadening study of the trivalent lanthanide-ion series. I. Line broadening as a probe of the electron-phonon coupling strength, *Physical Review B – Condensed Matter and Materials Physics* **55** (1997), 173 – 179, DOI: 10.1103/PhysRevB.55.173.

[7] L. Fan, Y. Shi, J. Xu, J. Xie and F. Lei, Consolidation of translucent Ce^{3+}-doped Lu_2SiO_5 scintillation ceramics by pressureless sintering, *Journal of Materials Research* **29** (2014), 2252 – 2259, DOI: 10.1557/jmr.2014.167.

[8] L. Guerbous and O. Krachni, The 4f-5d luminescence transitions in cerium-doped LuF_3, *Journal of Modern Optics* **53** (2006), 2043 – 2053, DOI: 10.1080/09500340600792424.

[9] L. Guerbous, M. Derbal and J. P. Chaminade, Photoluminescence and energy transfer of Tm^{3+} doped LiIn $(WO_4)_2$ blue phosphors, *Journal of Luminescence* **130** (2010), 2469 – 2475, DOI: 10.1016/j.jlumin.2010.08.014.

[10] M. S. E. Hamroun, L. Guerbous and A. Bensafi, Luminescent spectroscopy and structural properties of Ce^{3+}-doped low-temperature X_1–Y_2SiO_5 material prepared by polymer-assisted sol–gel method, *Applied Physics A* **122** (2016), Article number: 321, DOI: 10.1007/s00339-016-9790-7.

[11] M. S. E. Hamroun, L. Guerbous and A. Bensafi, Photoluminescence spectroscopy and structural characterization of Ce^{3+}-doped LYSO nanocrystalline powders, *Optik* **158** (2018), 1548 – 1552, DOI: 10.1016/j.ijleo.2018.01.034.

[12] T. M. Henderson, J. Paier and G. E. Scuseria, Accurate treatment of solids with the HSE screened hybrid, *Physica Status Solidi* (b) **248** (2011), 767 – 774, DOI: 10.1002/pssb.201046303.

[13] B. G. Janesko, T. M. Henderson and G. E. Scuseria, Screened hybrid density functionals for solid-state chemistry and physics, *Physical Chemistry Chemical Physics* **11** (2009), 443 – 454, DOI: 10.1039/B812838C.

[14] G. E. Jellison Jr., E. D. Specht, L. A. Boatner, D. J. Singh and C. L. Melcher, Spectroscopic refractive indices of monoclinic single crystal and ceramic lutetium oxyorthosilicate from 200 to 850 nm, *Journal of Applied Physics* **112** (2012), 063524, DOI: 10.1063/1.4752421.

[15] B. Kahouadji, L. Guerbous, A. Boukerika, S. D. Dolic, D. J. Jovanovi and M. D. Dramicanin, Sol gel synthesis and pH effect on the luminescent and structural properties of YPO_4: Pr^{3+} nanophosphors, *Optical Materials* **70** (2017), 138 – 143, DOI: 10.1016/j.optmat.2017.05.027.

[16] M. Kitaura, S. Tanaka and M. Itoh, Optical properties and electronic structure of Lu_2SiO_5 crystals doped with cerium ions: Thermally-activated energy transfer from host to activator, *Journal of Luminescence* **158** (2015), 226 – 230, DOI: 10.1016/j.jlumin.2014.10.010.

[17] G. Kresse and J. Furthmuller, Efficiency of ab-initio total energy calculations for metals and semiconductors using a plane-wave basis set, *Computational Materials Science* **6** (1996), 15 – 50, DOI: 10.1016/0927-0256(96)00008-0.

[18] G. Kresse and J. Hafner, Ab initio molecular dynamics for liquid metals, *Physical Review B – Condensed Matter and Materials Physics* **47** (1993), 558(R), DOI: 10.1103/PhysRevB.47.558.

[19] L. Lamiri, L. Guerbous, M. Samah, A. Boukerika and S. Ouhenia, Structural, morphological and steady state photoluminescence spectroscopy studies of red Eu^{3+}-doped Y_2O_3 nanophosphors prepared by the sol-gel method, *Luminescence* **30** (2015), 1336 – 1343, DOI: 10.1002/bio.2903.

[20] B. Liu, C. Shi, M. Yin, Y. Fu, G. Zhang and G. Ren, Luminescence and energy transfer processes in Lu_2SiO_5: Ce^{3+} scintillator, *Journal of Luminescence* **117**(2) (2006), 129 – 134, DOI: 10.1016/j.jlumin.2005.04.013.

[21] Q. Lu, Q. Liu, Q. Wei, G. Liu and J. Zhuang, Preparation and characterization of Lu_2SiO_5: Ce^{3+} luminescent ceramic fibers via electrospinning, *Ceramics International* **39** (2013), 8159 – 8164, DOI: 10.1016/j.ceramint.2013.03.090.

[22] C. Mansuy, C. Dujardin, R. Mahiou and J. M. Nedelec, Characterization and scintillation properties of sol–gel derived Lu_2SiO_5: Ln^{3+} (Ln = Ce, Eu and Tb) powders, *Optical Materials* **31** (2009), 1334 – 1336, DOI: 10.1016/j.optmat.2008.10.008.

[23] C. L. Melcher and J. S. Schweitzer, A promising new scintillator: cerium-doped lutetium oxyorthosilicate, *Nuclear Instruments and Methods in Physics Research Section A: Accelerators, Spectrometers, Detectors and Associated Equipment* **314** (1992), 212 – 214, DOI: 10.1016/0168-9002(92)90517-8.

[24] C. L. Melcher and J. S. Schweitzer, *Method of growing lutetium aluminum perovskite crystals and apparatus including lutetium aluminum perovskite crystal scintillators*, U.S. Patents 4,958,080; 5,-025,151; 5,660,627.

[25] J. D. Naud and T. A. Tombrello, C. L. Melcher and J. S. Schweitzer, The role of cerium sites in the scintillation mechanism of LSO, *IEEE Transactions on Nuclear Science* **43** (1996), 1324 – 1328, DOI: 10.1109/23.507059.

[26] L. Pidol, A. Kahn-Harari, B. Viana, E. Virey, B. Ferrand and P. Dorenbos, High efficiency of lutetium silicate scintillators, Ce-doped LPS, and LYSO crystals, *IEEE Transactions on Nuclear Science* **51** (2004), 1084 – 1087, DOI: 10.1109/TNS.2004.829542.

[27] L. Pidol, O. Guillot-Noël, A. Kahn-Harari, B. Viana, D. Pelenc and D. Gourier, EPR study of Ce^{3+} ions in lutetium silicate scintillators $Lu_2Si_2O_7$ and Lu_2SiO_5, *Journal of Physics and Chemistry of Solids* **67** (2006), 643 – 650, DOI: 10.1016/j.jpcs.2005.10.175.

[28] F. Rey-García, N. Ben Sedrine, A. J. S. Fernandes, T. Monteiro and F. M. Costa, Shifting Lu_2SiO_5 crystal to eutectic structure by laser floating zone, *Journal of the European Ceramic Society* **38** (2018), 2059 – 2067, DOI: 10.1016/j.jeurceramsoc.2017.11.003.

[29] P. C. Ricci, D. Chiriu, C. M. Carbonaro, S. Desgreniers, E. Fortin and A. Anedda, Pressure effects in lutetium yttrium oxyorthosilicate single crystals, *Journal of Raman Spectroscopy* **39** (2008), 1268 – 1275, DOI: 10.1002/jrs.1986.

[30] S.-Q. Shen, Q. Ma, Z.-B. Xu, J.-J. Xie, Y. Shi, J. Wang and F. Ai, Fabrication, structure and luminescence properties of polycrystalline Tb^{3+}-doped Lu_2SiO_5 films by Pechini sol–gel method, *Applied Surface Science* **258** (2011), 1768 – 1771, DOI: 10.1016/j.apsusc.2011.10.041.

[31] D.-Y. Shin, G. Cao and K.-N. Kim, Preparation and photoluminescence properties of Ce doped lutetium silicate nanopowders by sol-gel method, *Current Applied Physics* **11** (2011), S309 – S312, DOI: 10.1016/j.cap.2010.11.028.

[32] M. Taibeche, L. Guerbous, A. Boukerika, M. Kechouane, R. Nedjar and T. Zergoug, Ab-initio simulations at the atomic scale of an exceptional experimental photoluminescence signal observed in Ce^{3+}-doped Y_2O_3 sesquioxide system, *Optik* **127** (2016), 10561 – 10568, DOI: 10.1016/j.ijleo.2016.08.092.

[33] Y. K. Voron'ko, A. A. Sobol, V. E. Shukshin, A. I. Zagumennyi, Y. D. Zavartsev, S. A. Koutovoi, Spontaneous Raman spectra of the crystalline, molten and vitreous rare-earth oxyorthosilicates, *Optical Materials* **33** (2011), 1331 – 1337, DOI: 10.1016/j.optmat.2011.03.021.

[34] Y. K. Voron'koa, A. A. Sobol', V. E. Shukshina and Ya. V. Gerasimov, Spontaneous Raman scattering of $Lu_2Si_2O_7$ single crystals at temperatures in the range from 20 to 2173 K, *Physics of the Solid State* **57** (2015), 1424 – 1430, DOI: 10.1134/S1063783415070367.

[35] Y. Wang and P. D. Townsend, Common mistakes in luminescence analysis, *Journal of Physics: Conference Series* **398** (2012), 012003 (1-7), DOI: 10.1088/1742-6596/398/1/012003.

[36] G. K. Williamson and W. H. Hall, X-ray line broadening from filed aluminum and wolfram, *Acta Metallurgica* **1** (1953), 22 – 31, DOI: 10.1016/0001-6160(53)90006-6.

[37] L. Zheng, G. Zhao, C. Yan, X. Xu, L. Su, Y. Dong and J. Xu, Raman spectroscopic investigation of pure and ytterbium-doped rare earth silicate crystals, *Journal of Raman Spectroscopy* **38** (2007), 1421 – 1428, DOI: 10.1002/jrs.1789.

[38] Yu. Zorenko, M. Nikl, V. Gorbenko, V. Savchyn, T. Voznyak, R. Kucerkova, O. Sidletskiy, B. Grynyov, A. Fedorov, Growth and luminescent properties of Lu_2SiO_5 and Lu_2SiO_5:Ce single crystalline films, *Optical Materials* **33** (2011), 846 – 852, DOI: 10.1016/j.optmat.2011.01.004.